Acta Crystallographica Section D
Biological Crystallography
ISSN 0907-4449

Structure of *Escherichia coli* aminopeptidase P in complex with the inhibitor apstatin

Stephen C. Graham,[a] Megan J. Maher,[a] William H. Simmons,[b] Hans C. Freeman[a] and J. Mitchell Guss[a]*

[a]School of Molecular and Microbial Biosciences, University of Sydney, NSW 2006, Australia, and [b]Division of Biochemistry, Department of Cell Biology, Neurobiology and Anatomy, Loyola University Chicago Stritch School of Medicine, Maywood, IL 60153, USA

Correspondence e-mail: m.guss@mmb.usyd.edu.au

Received 2 June 2004
Accepted 30 July 2004

PDB Reference: aminopeptidase P–apstatin complex, 1n51, r1n51sf.

Aminopeptidase P (APPro) is a metalloprotease whose active site includes a dinuclear manganese(II) cluster. The enzyme cleaves the N-terminal residue from a polypeptide when the second residue is proline. A complex of *Escherichia coli* APPro (*Ec*APPro) with an inhibitor, apstatin [*N*-(2*S*,3*R*)-3-amino-2-hydroxy-4-phenyl-butanoyl-L-prolyl-L-prolyl-L-alaninamide], has been crystallized. Apstatin binds to the active site of *Ec*APPro with its N-terminal amino group coordinated to one of the two Mn^{II} atoms at the metal centre. The apstatin hydroxyl group replaces a hydroxide ion which bridges the two metal atoms in the native enzyme. The first proline residue of apstatin lies in a small hydrophobic cleft. The structure of the apstatin–*Ec*APPro complex has been refined at 2.3 Å resolution with residuals $R = 0.179$ and $R_{\rm free} = 0.204$. The structure of the complex illustrates how apstatin inhibits APPro and suggests how substrates may bind to the enzyme, but the basis of the proline-specificity remains elusive.

1. Introduction

Aminopeptidases catalyze the removal of the N-terminal residues of protein and peptide substrates. They are found in all three kingdoms of life and are thought to be involved in diverse functions including hormone regulation, protein maturation and the terminal degradation of proteins. Many aminopeptidases are specific for the N-terminal residue of their target peptide. For example, methionine aminopeptidase (MetAP) preferentially cleaves the N-terminal methionine residues from newly synthesized bacterial proteins, while leucine aminopeptidase (LeuAP) preferentially cleaves peptides with an N-terminal leucine residue. Most organisms have evolved special peptidases or proteases to deal with two problems: the need to recognize N-terminal residues and the fact that proline residues form secondary (—CO—N*R*—) rather than primary (—CO—NH—) amide bonds (Yaron & Naider, 1993). Aminopeptidase P (APPro; EC 3.4.11.9) is a peptidase that removes the N-terminal amino-acid residue from a peptide chain in which the second residue is proline (Yaron & Berger, 1970). APPro has been identified and isolated from organisms ranging from bacteria to mammals (Dehm & Nordwig, 1970; Yaron & Berger, 1970). In mammals, two isoforms have been isolated. They differ with respect to their sequence and their cellular localization. One is membrane-bound (Hooper *et al.*, 1990; Ryan, Denslow *et al.*, 1994; Simmons & Orawski, 1992) and the other is soluble (cytosolic; Harbeck & Mentlein, 1991; Rusu & Yaron, 1992; Vanhoof *et al.*, 1992).

It has been proposed that APPros have a range of biological functions ranging from the provision of proline for protein synthesis in bacteria to the regulation of hormones in mammals. Many biologically active polypeptides, including

coagulants, enzymes, growth factors, hormones, kinins, neurotransmitters and toxins, have an N-terminal Xaa-Pro sequence and may be substrates for APPro (Yaron, 1987), although specific involvement of APPro has been shown in only a few cases. For example, membrane-bound APPro (mAPPro) has been implicated in the inactivation of the nonapeptide hormone bradykinin, cleaving the N-terminal Arg-Pro bond (Simmons & Orawski, 1992). The inactivation of bradykinin is clinically important in humans, since the hormone is a potent vasodilator and cardioprotectant (Bhoola *et al.*, 1992; Linz *et al.*, 1995). Under conditions of myocardial ischaemia, bradykinin reduces the size of myocardial infarcts (Martorana *et al.*, 1990) and assists in reperfusion by acting as a vasodilator (Linz *et al.*, 1990; Zhu *et al.*, 1995). Membrane-bound APPro and angiotensin converting enzyme (ACE), which cleaves the Pro-Phe bond of bradykinin, are completely responsible for the degradation of bradykinin in the blood vessels of the heart and lungs of the rat (Ersahin & Simmons, 1997; Prechel *et al.*, 1995; Ryan, Berryer *et al.*, 1994).

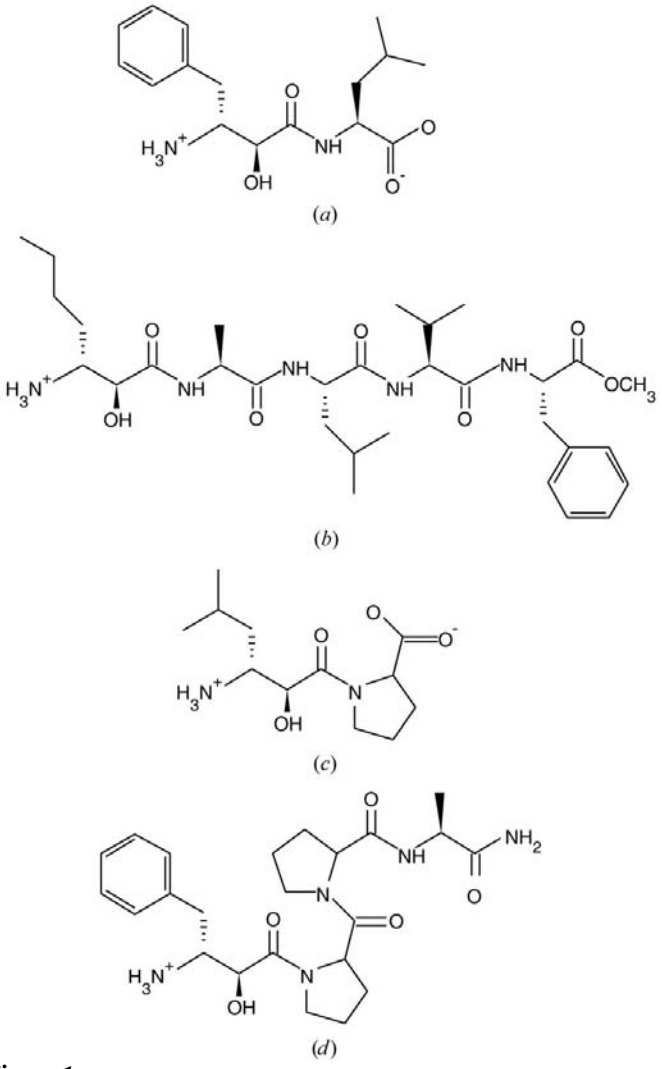

Figure 1
Aminopeptidase inhibitors. (*a*) Bestatin, *N*-(2*S*,3*R*)-3-amino-2-hydroxy-4-phenyl-butanoyl-L-Leu. (*b*) AHHpA-peptide, *N*-(2*S*,3*R*)-3-amino-2-hydroxy-heptanoyl-L-Ala-L-Leu-L-Val-L-Phe-OMe. (*c*) AHMH-Pro, *N*-(2*S*,3*R*)-3-amino-2-hydroxy-5-methyl-hexanoyl-L-Pro. (*d*) Apstatin, *N*-(2*S*,3*R*)-3-amino-2-hydroxy-4-phenyl-butanoyl-L-Pro-L-Pro-L-Ala-NH_2.

A number of inhibitors of aminopeptidases have been developed with the ultimate aim of producing therapeutic agents. For example, MetAP inhibitors are good candidates as antibacterial drugs since bacteria require MetAP for maturation of their own proteins (Vaughan *et al.*, 2002). Bestatin [(2*S*,3*R*)-3-amino-2-hydroxy-4-phenyl-butanoyl-L-leucine; Fig. 1] and amastatin [(2*S*,3*R*)-3-amino-2-hydroxy-5-methyl-hexanoyl-L-valyl-L-valyl-L-aspartate] are potent non-covalent inhibitors of aminopeptidases (Aoyagi *et al.*, 1978; Nakamura *et al.*, 1976).

Apstatin [(2*S*,3*R*)-3-amino-2-hydroxy-4-phenyl-butanoyl-L-prolyl-L-prolyl-L-alaninamide; Fig. 1] was designed to be an inhibitor of APPro by incorporating the required proline-specificity in the chemical framework of bestatin and amastatin (Prechel *et al.*, 1995). Like bestatin and amastatin, apstatin mimics the peptide substrates of the enzyme, but differs from normal peptides by having a 1,2-substituted β-aminoacyl N-terminal residue, $NH_2-CHR-CHOH-CO-$ ($R = -CH_2-C_6H_5$). As will be seen later, the $-CHOH-$ group plays an essential role in preventing the cleavage of the peptide group between the first and second residues. *In vivo*, apstatin is a promising cardiovascular therapeutic agent (Ersahin *et al.*, 1999; Kim *et al.*, 2000; Kitamura *et al.*, 1999; Wolfrum *et al.*, 2001). For example, administration of apstatin in combination with the ACE inhibitor ramiprilat blocks completely the degradation of bradykinin in isolated lung tissue (Prechel *et al.*, 1995). Apstatin is more effective as an inhibitor of the human membrane-bound form of APPro ($K_i = 0.64\ \mu M$) than it is towards the *Escherichia coli* enzyme ($K_i = 14\ \mu M$) (Prechel *et al.*, 1995).

APPro was originally isolated and characterized in *E. coli* (Yaron & Mlynar, 1968) and was later cloned and over-expressed (Yoshimoto *et al.*, 1988). At present, the only structurally characterized APPro is the *E. coli* enzyme (*Ec*APPro; Graham *et al.*, 2003; Wilce *et al.*, 1998). *Ec*APPro is a tetramer, or more correctly a dimer of dimers, in solution and in three different crystalline forms (Fig. 2; Graham *et al.*, 2003; Wilce *et al.*, 1998). The protomer has two domains. The N-terminal domain (residues 1–166) is joined by a short helical linker (residues 167–174) to the larger C-terminal domain (residues 175–440). The dinuclear manganese(II) centre is located in a depression on the inner concave surface of the β-sheet of the C-terminal domain. This C-terminal domain has a similar amino-acid sequence to domains of two other aminopeptidases: MetAP and prolidase (Fig. 3). Structural studies have shown the 'pita-bread' fold (Lowther & Matthews, 2002) of this domain to be conserved among these three enzymes (Bazan *et al.*, 1994; Maher *et al.*, 2004; Wilce *et al.*, 1998).

In native EcAPPro the active-site Mn^{II} atoms are bridged by a light atom, which is assumed to be a μOH^- ion (Wilce *et al.*, 1998). The environments of the two Mn^{II} atoms are different (Graham *et al.*, 2003). Mn_A is five-coordinate with a distorted square-pyramidal geometry, whereas Mn_B is six-

coordinate with a distorted octahedral geometry. Mn_A is coordinated by three O(carboxylate) atoms from Asp and Glu residues, an $N^{\varepsilon 2}$ (imidazole) atom from a His residue and the μOH^- ion. The donor atoms at Mn_B are four O(carboxylate) atoms from Asp and Glu residues, an H_2O molecule and the μOH^- ion. It has been proposed that the μOH^- ion, which also occurs in other peptidases with dinuclear metal centres, is the nucleophile that attacks the substrate's scissile peptide bond (Lowther & Matthews, 2002; Maher *et al.*, 2004; Wilce *et al.*, 1998). The identification of the bridging solvent as a μOH^- ion is consistent with the observation that the optimal pH for the enzyme activity is 8.3 (Kim *et al.*, 2000; Wilce *et al.*, 1998; Yaron & Berger, 1970).

Prior to the present work, the only structural information concerning the interaction between *Ec*APPro and a substrate or inhibitor came from the structure of the enzyme complexed with a dipeptide, Pro-Leu (L-prolyl-L-leucine). This dipeptide not only acts as an inhibitor but also represents the product that would be formed by the hydrolysis of a tripeptide, Xaa-Pro-Leu. Thus, the Pro-Leu complex of *Ec*APPro allows one to infer a possible location for the substrate in an enzyme–substrate complex. On the other hand, the structure of the complex reveals no close contacts between the enzyme and the inhibitor proline ring, so that the proline-specificity of the enzyme remains unexplained (Wilce *et al.*, 1998). In order to improve our understanding of the mechanism and specificity of *Ec*APPro, we have now determined the structure of the enzyme in a complex with apstatin.

2. Experimental

2.1. Crystallization of the native enzyme and preparation of an inhibitor complex

*Ec*APPro was overexpressed and purified as described previously (Wilce *et al.*, 1998; Zhang *et al.*, 1998). APPro was overexpressed in *E. coli* AN1459/pPL670. The cell lysate was subjected to ammonium sulfate precipitation and centrifugation. The pellet was resuspended and run on a DEAE-Fractogel column (Merck). The fraction containing APPro was then passed over a ceramic hydroxyapatite column (Bio-Rad). The protein was concentrated prior to crystallization. The inhibitor apstatin was synthesized as reported previously (Prechel *et al.*, 1995).

Crystals of the tetragonal crystal form of *Ec*APPro were grown with minor modifications to the published conditions. Crystals (space group $I4_122$, unit-cell parameters $a = 139.3$, $c = 231.0$ Å) were grown at 277 K by vapour diffusion in 6 µl hanging drops containing a 1:1 mixture of protein (8.7 mg ml^{-1}) and reservoir solution [0.2 *M* magnesium acetate, 0.1 *M* sodium cacodylate pH 6.8 and 25% methylpentanediol (MPD)]. The crystals retained good diffracting properties for more than a year. The apstatin complex was prepared by transferring crystals to a new hanging drop containing 4.5 µl 30% MPD, 2 µl 10 m*M* $MnCl_2$ and 0.5 µl 50 m*M* apstatin. The new drops were allowed to equilibrate overnight at 277 K. As the crystals were grown from solutions containing MPD, no cryoprotectant was required for flash-freezing. Within the limits of precision, the unit-cell parameters were identical to those of crystals of the native protein (Table 1).

2.2. Data collection and refinement

X-ray diffraction data for the apstatin–APPro complex were recorded with an R-AXIS IIc imaging-plate detector mounted on a Rigaku RU-200 rotating-anode generator.

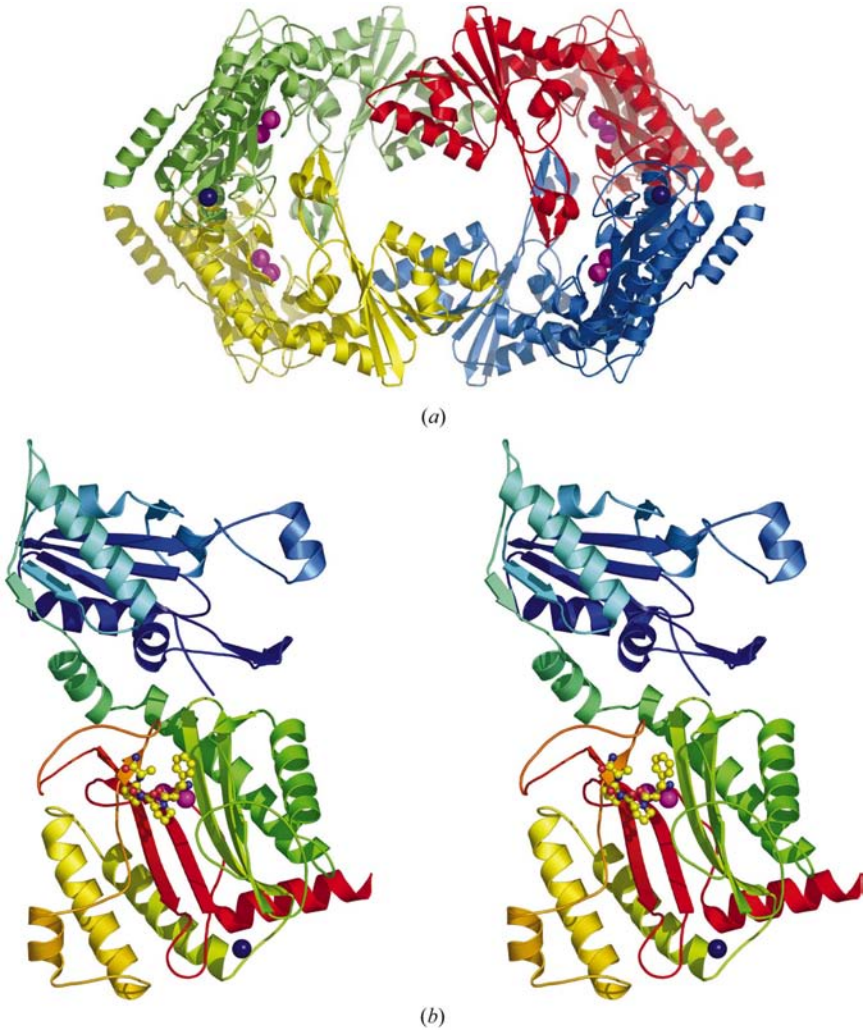

Figure 2
Structure of *Ec*APPro. (*a*) Tetramer with each monomer shown in a different colour. Mn^{II} atoms are shown as magenta spheres (active site) and a blue sphere (exogenous metal atom). (*b*) Stereoview of one monomer. Colours are ramped from blue at the N-terminus to red at the C-terminus. The polypeptide is drawn as a ribbon, with the inhibitor apstatin shown as a ball-and-stick model.

X-rays (Cu $K\alpha$, λ = 1.5418 Å) were collimated and focused with Yale mirrors (MSC, The Woodlands, USA). Crystals were flash-cooled in a stream of nitrogen gas at 113 K. The structure was refined using the structure of tetragonal *Ec*APPro (Wilce *et al.*, 1998) as a starting model, with the solvent molecules and metal atoms being omitted. The data-collection and refinement statistics are given in Table 1.

Rigid-body refinement was followed by positional refinement and grouped temperature-parameter refinement, starting with data at 4.0 Å resolution and gradually increasing the resolution to 2.8 Å. The active-site Mn^{II} atoms, which had been omitted from the original model, could be identified as positive peaks with amplitude greater than 10σ in $(F_{obs} - F_{calc})$ difference Fourier syntheses. Following addition of the Mn^{II} atoms to the active site, the model was subjected to a cycle of torsion-angle molecular-dynamics simulated annealing from 2500 K and unrestrained grouped *B*-value refinement using data to 2.8 Å. After several rounds of model building, including the manual assignment of solvent molecules interspersed with positional refinement and restrained individual *B*-value refinement using data to 2.3 Å, the residuals *R* and R_{free} were 0.186 and 0.208, respectively.

Throughout the refinement, the electron density for three regions of the polypeptide chain (residues 66–72, 82–90 and the C-terminal residues 439–440) remained weak. This was attributed to disorder, possibly indicating above-average flexibility. The electron density for these regions was not sufficiently well resolved to permit the modelling of alternate conformers. A single conformer for these sections of polypeptide was refined with atomic occupancies of 1.0, which resulted in temperature parameters >80 $Å^2$, consistent with disorder.

At this stage, three significant and persistent regions of positive electron-density difference were noted. (i) One large positive electron-density difference feature near the side chain of Glu396 was interpreted as a metal atom, being surrounded by a geometrically plausible arrangement of six potential ligand atoms. Mn^{II} and Mg^{II}, two metal species present in the crystallization buffer, can readily adopt such an octahedral arrangement. Mn^{II} exhibits significant anomalous signal when illuminated by Cu $K\alpha$ radiation ($f'' = 2.9\ e^-$), whereas the anomalous signal of Mg^{II} ($f'' = 0.2\ e^-$) is almost negligible, being less than that of sulfur ($f'' = 0.6\ e^-$). An anomalous difference Fourier synthesis was calculated and a peak with amplitude greater than 18σ, more than three times the amplitude of the highest peak present from an S atom (5.5σ at the S^{δ} atom of Met434), was present at the position of the putative metal atom. The amplitude of this anomalous peak was comparable with the anomalous peaks present at the positions of the two active-site metal atoms (11.6σ and 22.3σ for Mn_A and Mn_B, respectively) and the metal atom was therefore modelled as Mn^{II}. The atom is probably an artifact of crystallization. It is distant from the active site and makes contacts with more than one tetramer. (ii) Persistent positive electron-density difference was also observed at the thiol group of Cys249. The hypothesis that the thiol (−SH) group was partially oxidized to sulfenate (−SOH) was tested by adding an O atom with partial occupancy at the appropriate position, but this O atom inevitably acquired an unacceptably high temperature factor during further refinement. The residual difference electron density is unlikely to be functionally significant since Cys249 is on the solvent-accessible

```
HscAPPro   1 PICIAKAVKNSAESEGMRRAHIKDAVALCELFNWLEKEVPKGGVTEISAADKAEEFRRQQADFV---DLSFP
HsmAPPro 349 PVMMTKAVKNSKEQALLKASHVRDAVAVIRYLVWLEKNVPKGTVDEFSGAEIVDKFRGEEQFSS---GPSFE
PfProl   117 VIKDLRIIKTKEEIEIIEKACEIADKAVMAAIEEITEGKREREVAAKVEYLMKMNGAE---------KPAFD
EcAPPro  168 VVHEMRLFKSPEEIAVLRRAGEITAMAHTRAMEKCRPGMFEYHLEGEIHHEFNRHGAR---------YPSYN
EcMetAP    1 ---MAISIKTPEDIEKMRVAGRLAAEVLEMIEPYVKPGVSTGELDRICNDYIVNEQHAVSACLGYHGYPKSV

HscAPPro  70 TISSTGPNGAIIHYAPVPETNRTLSLDEVYLIDSGAQYKDGTTDVTRTMHF-GTPTAYEKECFTYVLKGHIA
HsmAPPro 418 TISASGLNAALAHYSPTKELNRKLSSDEMYLLDSGGQYWDGTTDITRTVHW-GTPSAFQKEAYTRVLIGNID
PfProl   180 TIIASGHRSALPHGVASDKRI---ERGDLVVIDLGALYNHYNSDITRTIVV-GSPNEKQREIYEIVLEAQKR
EcAPPro  231 TIVGSGENGCILHYTENECEM---RDGDLVLIDAGCEYKGYAGDITRTFPVNGKFTQAQREIYDIVLESLET
EcMetAP   70 CISINEV---VCHGIPDDAKL--LKDGDIVNIDVTVIKDGFHGDTSKMFIV-GKPTIMGERLCRITQESLYL

HscAPPro 141 VSAAVFPTGTKGHLLDSFARSALWD-------------------SGLDYLHGTGHGVGSFLNVHEGPCGISY
HsmAPPro 489 LSRLIFPAATSGRMVEAFARRALWD-------------------AGLNYGHGTGHGIGNFLCVHEWPVGFQS
PfProl   248 AVEAAKPGMTAKELDSIAREIIKEYGY-----------------GDYFIHSLGHGVG--LEIHEWPRISQY
EcAPPro  300 SLRLYRPGTSILEVTGEVVRIMVSGLVKLGILKGDVDELIAQNAHRPFFMHGLSHWLG--LDVHDVGVYGQD
EcMetAP  136 ALRMVKPGINLREIGAAIQKFVEAE-------------------GFSVVREYCGHGIG--RGFHEEPQVLHY

HscAPPro 194 KTFSDE-PLEAGMIVTDEPGYYEDG-----------------AFGIRIENVVLVVPVKTKYNFN 239
HsmAPPro 542 NNIAMA----KGMFTSIEPGYYKDG-----------------EFGIRLEDVALVVEAKTKYPGS 584
PfProl   300 DETVLK----EGMVITIEPGIYIPK-----------------LGGVRIEDTVLITENGAKRLTK 342
EcAPPro  370 RSRILE----PGMVLTVEPGLYIAPDAEVPEQYR--------GIGIRIEDDIVITETGNENLTA 421
EcMetAP  187 DSRETNVVLKPGMTFTIEPMVNAGKKEIRTMKDGWTVKTKDRSLSAQYEHTIVVTDNGCEILTL 250
```

Figure 3
Alignment of the sequences of the catalytic domains of *Hs*cAPPro, *Hs*mAPPro, *Pf*Prol, *Ec*APPro and *Ec*MetAP. Strictly conserved residues are coloured blue and conservatively substituted residues are coloured yellow. * denotes metal ligands and # denotes other residues that are important for catalysis (His243 and His361 in *Ec*APPro). Residues that interact with apstatin in *Ec*APPro (and equivalent residues) are shown in bold.

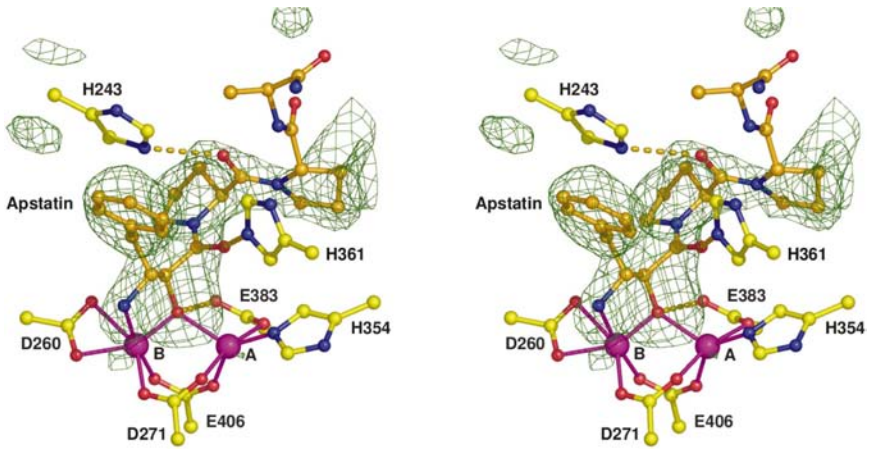

Figure 4
Stereoview of apstatin bound at the active site. The magenta spheres represent the Mn^{II} atoms. Only protein residues coordinating the metal atoms or forming hydrogen bonds with apstatin are shown. The 'omit' $F_o - F_c$ electron-density difference map calculated before apstatin was included in the model is contoured at 3σ.

Table 1
Crystallographic data and refinement statistics for the apstatin complex of *Ec*APPro.

Values in parentheses refer to the highest resolution shell (2.4–2.3 Å).

Space group	$I4_122$
Unit-cell parameters (Å)	a = 139.3, c = 231.0
Resolution range (Å)	20.0–2.3
Redundancy	2.6 (2.4)
$\langle I/\sigma(I)\rangle$	18.2 (2.0)
Completeness (%)	97.0 (96.2)
$R_{\rm merge}$†	4.4 (41.1)
No. reflections	48993 (5361)
$R_{\rm work}$‡	0.179 (0.299)
$R_{\rm free}$ (5% of data)	0.204 (0.333)
Average B values (Å^2)	
Protein	43.4
Solvent	51.6
ESU§ (Å)	0.17
No. atoms	
Protein	3499
Alternate conformer	31
Solvent	425
Ligand atoms	33
Metal ions	3
R.m.s. deviation from standard geometry	
Bond lengths (Å)	0.005
Bond angles (°)	1.2
Ramachandran plot statistics	
Residues in most favoured region (%)	92.2
Residues in additional allowed region (%)	7.5
Residues in generously allowed region (%)	0.3

† $R_{\rm merge} = \sum|I_h - \langle I_h\rangle|/\sum\langle I_h\rangle$. ‡ R values = $\sum|F_{\rm obs} - F_{\rm calc}|/\sum F_{\rm obs}$. § The estimated standard uncertainty (ESU) in the position of an average atom is stated as the Diffraction Precision Indicator (Cruickshank, 1999).

surface of the protein, far from the active site and from all inter-subunit interfaces. (iii) An extended region of positive difference electron density near the active-site metal atoms (Fig. 4) could be modelled as an apstatin molecule. The electron density beyond the first Pro residue of the molecule was weak and the two C-terminal residues and the C-terminal amide group were included in the model with zero occupancy.

A final round of positional and restrained B-factor refinement resulted in a structure with residuals R = 0.179 and $R_{\rm free}$ = 0.204.

2.3. Software

Diffraction data were integrated and scaled with *DENZO* and *SCALEPACK* (Otwinowski & Minor, 1997). Manual model adjustment was carried out with the program *O* (Jones *et al.*, 1991), using standard types of electron-density difference map. The program *CNS* (Brünger *et al.*, 1998) was used for the refinement calculations. The final model was validated by means of *PROCHECK* (Laskowski *et al.*, 1993) and *WHATCHECK* (Vriend, 1990). Structures were superposed using the program *LSQMAN* (Kleywegt & Jones, 1997). C^α-position difference plots were produced using *ESCET* (Schneider, 2002). Fig. 1 was produced using the program *XDrawChem* (http://xdrawchem.sourceforge.net). Figs. 2 and 4–7 were produced using the program *PyMol* (DeLano Scientific). Fig. 3 was produced using the program *BELVU* (http://www.cgb.ki.se/cgb/groups/sonnhammer/Belvu.html). Fig. 6 was produced using *HBPLUS* (McDonald & Thornton, 1994) and *LIGPLOT* (Wallace *et al.*, 1995).

3. Results

3.1. Structure of the apstatin–*Ec*APPro complex

The final refined structure comprises 3530 protein atoms (including 31 atoms in alternate conformers for residues Glu133, Arg302 and Arg399), 425 water molecules, three Mn^{II} atoms and 33 atoms (13 assigned zero occupancy) representing a molecule of apstatin. As previously discussed, three regions of the protein (residues 66–72, 82–90 and the C-terminal residues 439–440) are poorly ordered or mobile as indicated by weak electron density and high temperature factors. Residues 66–72 are in a loop that is completely exposed to the solvent, so that disorder can reasonably be expected. Residues 82–90 also lie in a loop, but here the apparent disorder is surprising since the loop makes several contacts with a symmetry-related monomer. The contacts include two hydrogen bonds, Ile87 O$\cdots$H—N LeuB242 and Trp88 O$\cdots$H—N HisB243.

3.2. The inhibitor-binding site

Apstatin is bound to APPro at the bottom of the active-site cleft (Fig. 2*b*). There are six bonding interactions between the inhibitor and the enzyme (Figs. 5*a* and 6). (i) The terminal N(amino) atom of apstatin coordinates the metal atom Mn_B, displacing a coordinating water molecule present in the native structure. (ii and iii) The hydroxyl group of apstatin (O1) replaces the bridging μOH^- ion between the active-site Mn^{II} atoms and forms bonds to both Mn atoms. (iv) In addition, the bridging hydroxyl group forms a hydrogen bond to the $O^{\varepsilon1}$(carboxylate) atom of Glu383. (v) The first O(amide) atom (O) of apstatin forms a short hydrogen bond, 2.6 Å, to the $N^{\varepsilon2}$ atom of His361. (vi) The second O(amide) atom of apstatin (O2) forms a hydrogen bond to the $N^{\varepsilon2}$ atom of His243. The imidazole ring of His243 is disordered in the structure of the native enzyme as indicated by the absence of 'omit' electron-density. When apstatin is bound there is significant but weak electron density for the side chain of this residue, indicating that it has at least one preferred conformer in the complex. A similar change in His243 occurs when the inhibitor Pro-Leu is bound (Wilce *et al.*, 1998).

In addition to these bonding interactions, apstatin makes a number of van der Waals contacts with the host molecule (Fig. 6). The side chain of the first (pseudo-Phe) residue makes contacts with the side chains of Val360, Tyr229, His361 and His243. Having bulky side chains that can adopt a variety of conformations, these residues form a flexible pocket defining the binding site for the N-terminal residue (Fig. 5*a*). The phenyl ring of apstatin is loosely stacked between the side chains of Tyr229 and His243. The proline ring of the second apstatin residue makes contacts with the polypeptide at His350 and Arg404 and the metal-ligand residue Glu383.

Residues from two neighbouring subunits in the tetramer define part of the active-site pocket in *Ec*APPro. [We use

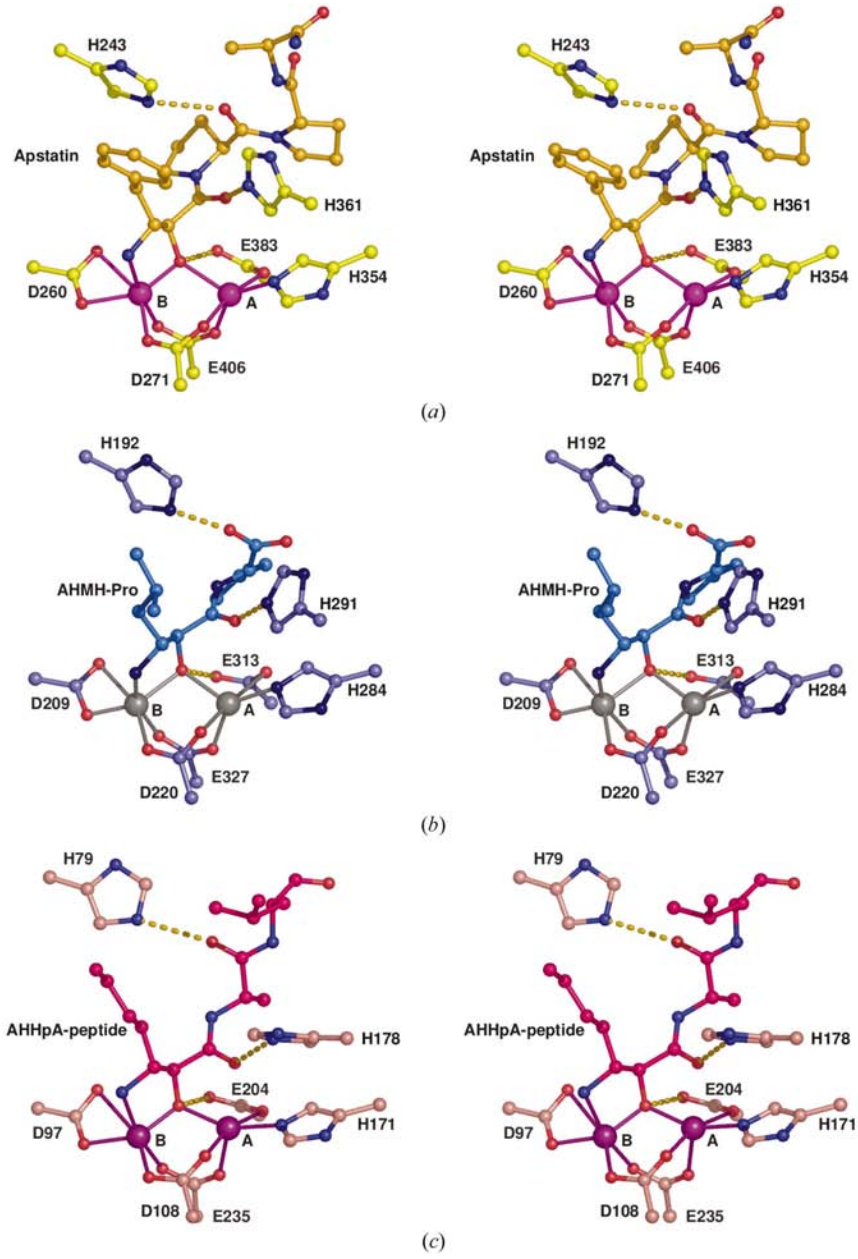

Figure 5
Stereoviews of the active sites in inhibitor complexes of aminopeptidases. (*a*) Apstatin complex of *Ec*APPro. Mn^{II} atoms are magenta. (*b*) AHMH-Pro complex of *Pf*Prol. Zn^{II} atoms are grey. (*c*) AHHpA-peptide complex of *Ec*MetAP. Co^{II} atoms are purple.

labels B and C to indicate atoms in the subunits at $(\frac{1}{2}-y, \frac{1}{2}-x, \frac{1}{2}-z)$ and at $(\frac{1}{2}+y, \frac{1}{2}+x, \frac{1}{2}-z)$, respectively, in relation to the unlabelled subunit at x, y, z]. A loop from AlaB37 to SerB39 lies above the N-terminal end of apstatin, the closest contact (4.0 Å) being between the C^{β} atom of SerB39 and the phenyl-ring C^{ζ} atom of apstatin. The two C-terminal residues of apstatin were not in sufficiently resolved electron density for refinement, but their approximate positions can be inferred. They protrude from the active site between ArgC153 on one side and a loop that includes TrpB88 and PheB89 on the other side. Residues TrpB88 and PheB89 help to define the boundary of the inhibitor-binding pocket. They are part of the loop at residues 82–90, the disorder of which has been mentioned above. The flexibility of the loop seems to be consistent with the ability of *Ec*APPro to accommodate a large range of biological substrates differing in length and sequence (Yoshimoto *et al.*, 1994).

3.3. Additional comments on the apstatin–*Ec*APPro structure

In agreement with the structure of *Ec*APPro in its orthorhombic crystal form (Graham *et al.*, 2003), the side chain of His350 in this structure is rotated by 180° about the $C^{\beta}-C^{\gamma}$ bond with respect to the orientation originally reported for the structures in the hexagonal and tetragonal crystal forms (Wilce *et al.*, 1998). In the revised orientation, the imidazole ring of His350 forms two strong hydrogen bonds, His350 $N^{\delta1}-H\cdots O$ Gly351 and His350 $N^{\varepsilon2}\cdots H-O^{\eta}$ Tyr387 (2.8 and 2.7 Å, respectively).

Another interesting interaction occurs at His217, which forms a 2.7 Å $N^{\delta1}\cdots H\cdots N^{\delta1}$ hydrogen bond to the corresponding residue, HisB217, in a neighbouring subunit. The two His residues are related by a twofold symmetry axis, so that the hydrogen bond between them must be disordered. In this respect, the structure of the apstatin–*Ec*APPro complex differs from the previously reported structure of the native protein. In the low-pH structure of APPro (PDB code 1jaw), the imidazole rings of the symmetry-related His217 residues are rotated so that the closest contact (3.5 Å) is between their $C^{\delta2}$ atoms. In the hexagonal and orthorhombic structures (PDB entries 1az9 and 1m35), the imidazole rings are rotated away from each other and a water molecule is located between them.

3.4. The inhibitor is bound without causing significant structural changes

The binding of apstatin causes only minor changes in the structure of *Ec*APPro. Within the limits of precision, the polypeptide backbone remains undisturbed. When the C^{α} atoms of a single subunit of the apstatin–APPro complex are superposed on the C^{α} atoms of the native APPro, the r.m.s. difference between the positions of corresponding atoms is 0.26 Å. (Residues 67–71, 82–90 and 439–440 are omitted from the superposition.) Since the ESU (the estimated uncertainty in the position of an average atom) in the apstatin complex is 0.17 Å, the r.m.s. difference is not significant.

The quaternary structure of the APPro tetramer likewise remains unperturbed when apstatin is bound. When tetramers of the apstatin complex and of the native protein are gener-

ated by applying the appropriate twofold symmetry operations to the respective monomers, superposition of the C^{α} atoms leads to an r.m.s. difference of 0.39 Å. Neither C^{α}-difference plots nor the positions of the monomer centroids within the tetramers (data not shown) indicate any concerted movement of the individual or assembled domains.

A similar conclusion is reached when the apstatin–APPro complex is superposed on the complex of APPro with another inhibitor, Pro-Leu. The r.m.s. differences for the monomer–monomer and tetramer–tetramer superpositions are then 0.27 and 0.44 Å, respectively. These r.m.s. differences are not significantly greater than the corresponding r.m.s. differences between the Pro-Leu complex and native APPro, being 0.13 and 0.15 Å, respectively (Graham *et al.*, 2003). The fact that both the inhibitors apstatin and Pro-Leu are bound to *Ec*APPro without any significant quaternary structural rearrangement is consistent with the lack of any evidence for allostery in the *E. coli* enzyme.

4. Discussion

4.1. Comparison between the complexes of *Ec*APPro with two inhibitors, apstatin and Pro-Leu

The inhibitor studied in the present work, apstatin, closely resembles a substrate of the enzyme APPro. A previous study dealt with the inhibitor Pro-Leu, a dipeptide that mimics the product that would be obtained by the reaction of the enzyme with a tripeptide substrate, Xaa-Pro-Leu (Wilce *et al.*, 1998). An important difference between the two inhibitor–*Ec*APPro complexes is that apstatin displaces the nucleophilic μOH^{-} ion from the dinuclear metal site, whereas Pro-Leu leaves the active site intact. Despite this, a superposition of the structures of the two complexes results in an insignificant r.m.s. difference between the positions of corresponding *Ec*APPro protein C^{α} atoms (see §3). In the same superposition, the first Pro ring in apstatin is displaced by about 0.8 Å with respect to the Pro ring in Pro-Leu (Fig. 7*a*). We assume that the Pro-Leu dipeptide is bound at the position that would be occupied by the C-terminal product of catalysis of an Xaa-Pro-Leu substrate. We furthermore assume that the Pro residue does not move significantly during catalysis, allowing us to infer the position of the Pro residue in a substrate Xaa-Pro-Leu before it is cleaved. The displacement of the Pro ring in apstatin from this inferred position is most likely a consequence of the presence of an additional group, —CHOH—, which lengthens the N-terminal residue and anchors the inhibitor to the active site. While the replacement of the nucleophilic μOH^{-} ion by the —CHOH— group alone accounts for the inhibitory effect of apstatin, it is noted that the scissile peptide bond is also further from the dinuclear metal centre than the position inferred from the Pro-Leu complex.

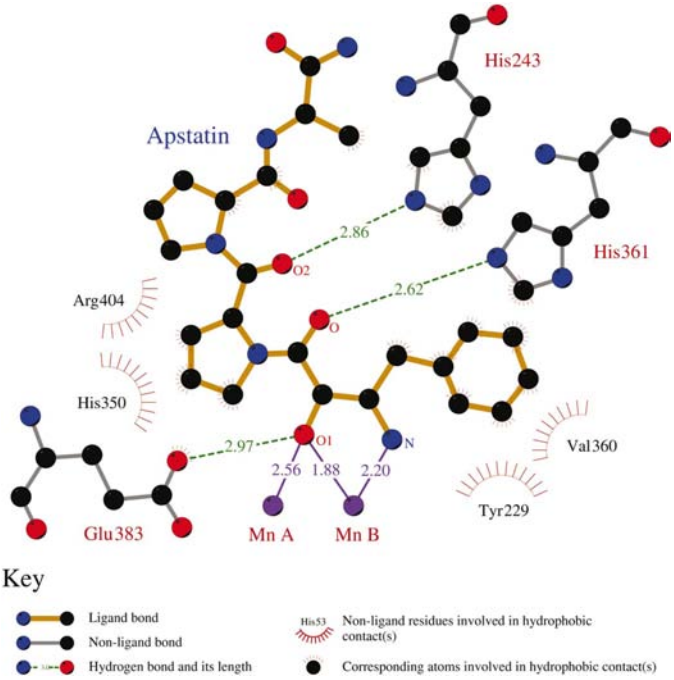

Figure 6
Two-dimensional schematic diagram showing the interactions between apstatin and *Ec*APPro. Hydrogen bonds (green dashed lines), inhibitor–metal ligand interactions (purple sticks) and hydrophobic interactions (red combs) are shown. Beyond the first (P_1') proline residue there is a shortage of interactions between the inhibitor and the protein.

4.2. Comparison between the apstatin–*Ec*APPro complex and an inhibitor–*Pf*Prol complex

The crystal structure of prolidase (*Pf*Prol), a metallopeptidase from the hyperthermophilic bacterium *Pyrococcus furiosus*, has recently been reported (Maher *et al.*, 2004). *Pf*Prol is closely related to *Ec*APPro in both structure and function. The catalytic domain of *Pf*Prol has a 'pita-bread' fold, an active site that includes a dinuclear metal centre bridged by a μOH^{-} ion, and metal-binding protein side chains and water molecules similar to those observed in *Ec*APPro. Both *Pf*Prol and *Ec*APPro have a preference for substrates that have Pro as the second residue (the P_1' position, according to the nomenclature of Schechter & Berger, 1967). An important difference is that the former has a strict requirement for dipeptide substrates, whereas the latter has a preference for oligopeptide substrates. The ability of the enzymes to distinguish between the two types of substrate has been attributed to a difference between the conformations of a single polypeptide loop (residues 291–300 in *Pf*Prol; residues 361–369 in *Ec*APPro; Maher *et al.*, 2004). The loop approaches the active site more closely in *Pf*Prol than in *Ec*APPro, thus restricting the length of the peptide substrate that can be accommodated (see Fig. 6 in Maher *et al.*, 2004).

The structure of an inhibitor complex of *Pf*Prol has been described (Fig. 5*b*; Maher *et al.*, 2004). The inhibitor in the complex is (2*S*,3*R*)-3-amino-2-hydroxy-5-methyl-hexanoyl-proline (AHMH-Pro), a close analogue of apstatin (Fig. 1). When the structures of the apstatin complex of *Ec*APPro and the AHMH-Pro complex of *Pf*Prol are compared (Fig. 7*b*), the pseudo-Leu side chain of AHMH-Pro and the pseudo-Phe side chain of apstatin occupy equivalent positions in relation to the metal centres. The pocket for the pseudo-Leu side chain in *Pf*Prol is defined by residues equivalent to those already

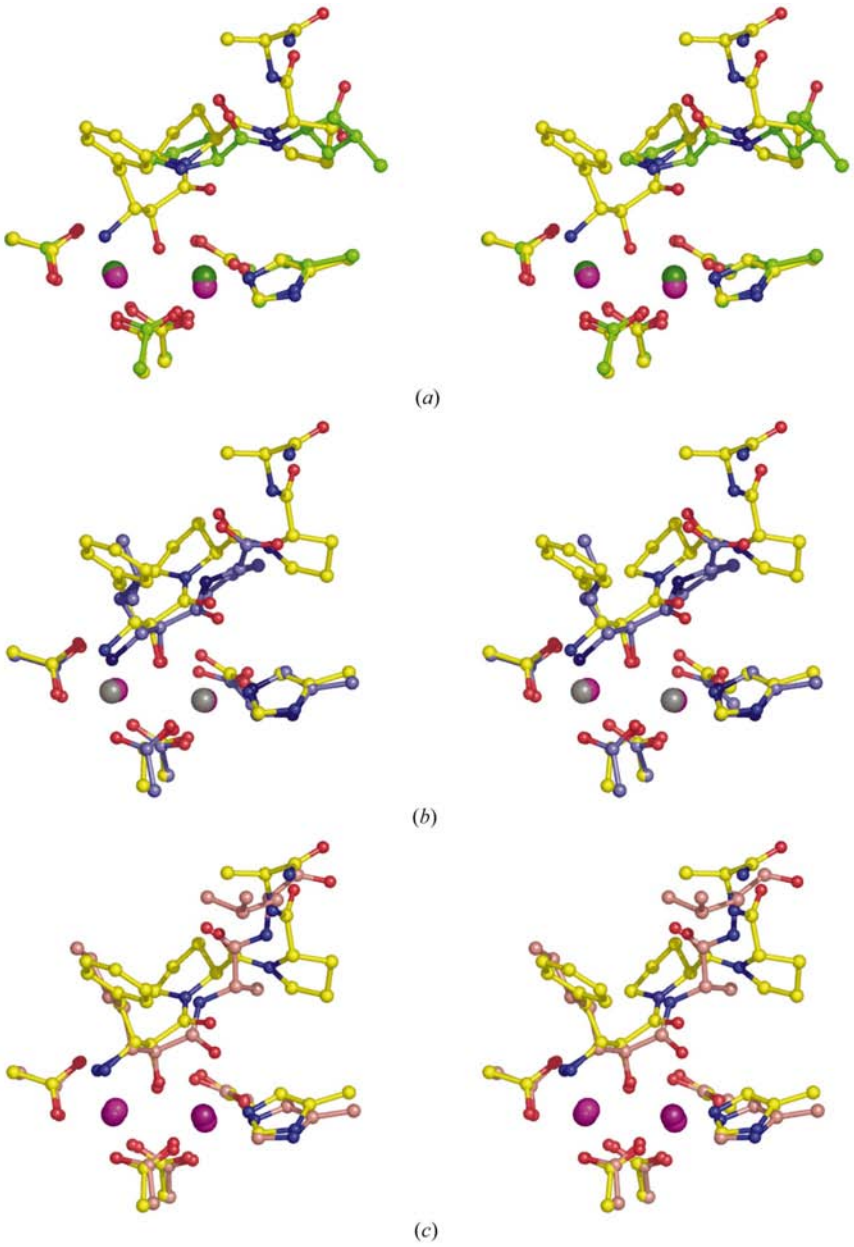

Figure 7
Stereoviews of pairwise superpositions of the active sites in inhibitor–aminopeptidase complexes. (*a*) Apstatin (yellow) and Pro-Leu (green) complexes of *Ec*APPro. (*b*) Apstatin complex of *Ec*APPro (yellow) and AHMH-Pro complex of *Pf*prol (blue). (*c*) Apstatin complex of *Ec*APPro (yellow) and AHHpA-peptide complex of *Ec*MetAP (pink).

described for *Ec*APPro, with the addition of a hydrophobic contact from LeuB37 in the neighbouring subunit of the *Pf*Prol dimer.

While the general positions of the second, specificity-conferring proline residues are similar, the positions of the prolidyl rings are sufficiently different so that the distance between the C^{γ} atoms is 2.0 Å. However, the *Ec*APPro residues His350, Glu383 and Arg404 that line the active site overlay perfectly with their equivalent residues in *Pf*Prol (His280, Glu313 and Arg325). The difference between the proline orientations in these two inhibitor complexes shows that the S_1' binding pockets of the enzymes permit considerable flexibility.

4.3. Comparison between the apstatin–*Ec*APPro complex and an inhibitor–*Ec*MetAP complex

*Ec*MetAP is a structurally characterized aminopeptidase that is a monomer in solution. It has a single domain that exhibits the 'pita-bread' fold and contains a dinuclear hydroxo-bridged metal site (Lowther *et al.*, 1999). Unlike APPros and prolidases, which require substrates with Pro as the second residue, MetAPs require that substrate peptides have an N-terminal Met residue. The requirement for the second residue is less strict, with Ala residues preferred but other residues such as Gly, Ser, Thr, Pro and Val able to be accommodated (Hirel *et al.*, 1989).

The structure of a complex of the enzyme with an inhibitor, (3*R*)-amino-(2*S*)-hydroxy-heptanoyl-L-Ala-L-Leu-L-Val-L-Phe-OMe (AHHpA-peptide; Fig. 1), has been reported (Fig. 5*c*; Lowther *et al.*, 1999). The inhibitor, designed to be an analogue of bestatin, inhibits *Ec*MetAP with an IC_{50} of 5 μ*M* (Keding *et al.*, 1998). In the structural analysis of the inhibitor–enzyme complex, convincing electron density was visible only for the N-terminal AHHpA-L-Ala-L-Leu portion of the inhibitor. When the structures of the apstatin complex of *Ec*APPro and the AHHpA–peptide complex of *Ec*MetAP are superposed and adjusted manually to optimize the overlap of the active-site metal-binding residues, excellent agreement is obtained (Fig. 7*c*). The terminal amino and hydroxyl groups of the inhibitor molecules coordinate the metal atoms and these interactions are identical within the limits of precision. The hexanoyl side chain of the first residue of AHHpA superposes closely on the $-CH_2-$Phe side chain of the first residue of apstatin; the aliphatic side chain of AHHpA actually parallels one edge of the benzyl group of apstatin. The aliphatic side chain of AHHpA mimics methionine and fits neatly into a tapered pocket in *Ec*MetAP. The residues that define the pocket are His79, Cys59, Cys70, Tyr62, Tyr65, Phe177 and Trp221 (Lowther *et al.*, 1999). The $-CH_2-$Phe side chain of apstatin lies in a much more open pocket in *Ec*APPro and makes few contacts with the host molecule. Thus, while *Ec*MetAP has a well defined P_1 binding pocket with specificity for Met, *Ec*APPro should accommodate a wider range of residues in this position. Activity assays against a wide range of substrates have shown this to be the case (Yoshimoto *et al.*, 1994).

However, while the N-terminal (P_1) residues of the inhibitors overlap well in the superposed inhibitor–enzyme

complexes, the second (P_1') residues have significantly different positions and orientations. The C^{α} atoms of the P_1' residues (the first Pro in apstatin and the Ala in the AHHpA-peptide) lie more than 2.2 Å apart. This large difference at the P_1' residues is associated with different values of the torsion angle φ (-85° at Pro in the apstatin complex, 105° at the Ala in the AHHpA-peptide complex) and with different orientations of the carbonyl bond in the scissile peptide group. Since conformations with an angle φ of 105° are not obtainable by Pro residues, one must conclude that Met-Pro-... substrates of *Ec*MetAP bind to the enzyme in a conformation different from that seen in the AHHpA–peptide complex and perhaps more similar to that seen in the complex of apstatin with *Ec*APPro.

4.4. Comments on the catalytic mechanism of 'pita-bread' aminopeptidases

The fact that the 'pita-bread' aminopeptidases (MetAP, prolidase and APPro) have similar polypeptide folds and active-site structures suggests that these enzymes also have similar modes of substrate binding and similar catalytic mechanisms (Copik *et al.*, 2003; Lowther & Matthews, 2002). This hypothesis is supported by the strong analogies between the structures of the three inhibitor–enzyme complexes discussed here.

A recent proposal for this common catalytic mechanism (scheme 4 of Lowther & Matthews, 2002) is as follows. The OH^- ion that bridges the active-site metal atoms acts as a nucleophile, attacking the carbonyl C atom of the scissile peptide bond of the substrate to form a tetrahedral oxyanion intermediate. This intermediate is stabilized by the bonds between the metal atoms and the OH^- ion, by an interaction between the metal atom *M*1 (Mn_A in *Ec*APPro) and the O(peptide) atom O_C, and by a hydrogen bond between O_C and the $N^{\varepsilon 2}$ atom of a His residue (His361 in *Ec*APPro, His291 in *Pf*Prol, His178 *Ec*MetAP). The pre-attack enzyme–substrate complex and the tetrahedral intermediate are further stabilized by a hydrogen bond between the N(peptide) atoms of the substrate P_1' residue and a second His residue (His243 in *Ec*APPro, His192 in *Pf*Prol, His79 in *Ec*MetAP). A direct interaction between the amino-terminus of the substrate and the second metal atom *M*2 (Mn_B in *Ec*APPro) may not be necessary for catalysis.

The direct interaction between *M*1 (Mn_A in *Ec*APPro) and O_C required in this mechanism is consistent with Mn_A having a distorted square-pyramidal coordination in the resting enzyme (Graham *et al.*, 2003). An interaction with O_C would lead to an octahedral geometry at Mn_A, presumably requiring less reorganization enthalpy than the displacement of an existing ligand if the metal were already six-coordinate. On the other hand, the stabilizing influence attributed to an N(peptide)—H···N(His) hydrogen bond (His243 in *Ec*APPro, His192 in *Pf*Prol, His79 in *Ec*MetAP) requires modification in the case of substrates where the N(peptide) atom belongs to a Pro residue. Proline residues have no proton attached to the N(peptide) to participate in the proposed hydrogen bond. There is little doubt that the cited His residue plays an important role in the catalytic reaction: it is conserved in all the 'pita-bread' fold aminopeptidases (Fig. 3) and in the case of *Ec*MetAP a mutation from His to Ala causes a serious reduction in the catalytic efficiency (Lowther *et al.*, 1999). The precise role of this His residue therefore requires further investigation.

5. Conclusions

Apstatin exerts its clinical effect by inhibiting the membrane-bound form of human APPro (*Hs*mAPPro). The homologous *E. coli* enzyme binds apstatin an order of magnitude less strongly, forming the inhibitor–enzyme complex presented in this paper. Comparison of the sequences of the human and *E. coli* enzymes (Fig. 3) shows that all *Ec*APPro residues shown to interact with the two ordered N-terminal residues of apstatin (Tyr229, His243, His350, Val360, His361, Glu383 and Arg404) are either strictly conserved or conservatively substituted in *Hs*mAPPro. Thus, we assume that the interactions observed between the two ordered residues of apstatin and *Ec*APPro will be conserved in complexes of apstatin with *Hs*mAPPro. The difference in the potency of inhibition is therefore likely to arise from specific interactions between *Hs*mAPPro and the two residues of apstatin that are not ordered in the *Ec*APPro complex. We propose that the source of this interaction is a loop (residues 362–367 in *Ec*APPro; residues 536–539 in *Hs*mAPPro) that adopts a different conformation in the two enzymes. Close inspection of the sequence alignment (Fig. 3) shows that the tetrapeptide sequence HDVG, residues 361–364 in *Ec*APPro, is HEXP in *Hs*mAPPro, *Pf*Prol and *Ec*MetAP. In the structures of *Pf*Prol and *Ec*MetAP the proline residue in this sequence adopts a *cis* configuration and the polypeptide loop that follows is folded down over the active site so that it forms part of the substrate-recognition pocket (Fig. 6 of Maher *et al.*, 2004; Lowther *et al.*, 1999). Given the conservation of this sequence, it is likely that the equivalent loop in *Hs*mAPPro also folds in towards the active site. This loop would then be in a position to interact with the portion of apstatin that is disordered in the *Ec*APPro complex, providing additional binding energy and thereby explaining why the human enzyme is inhibited more potently than the *E. coli* enzyme by apstatin.

The properties that the three 'pita-bread' inhibitor–enzyme complexes whose structures are now available have in common are the replacement of the bridging μOH^- ion at the dinuclear metal site by a —CHOH— group of the inhibitor and the coordination of one of the active-site metal atoms by the terminal NH_2 group of the inhibitor. The replacement of the μOH^- ion provides a sufficient reason why the enzyme is inhibited: the nucleophile required for the catalytic reaction is no longer there. The lesson to be learned from the coordination of the terminal NH_2 group to the metal site is less clear. A facile inference is that substrates also coordinate the metal atom and that this contributes to the preference for substrates with a free amino-terminus. Equally logical inferences are that the coordination of the NH_2 group is part of the inhibitory

effect, that the NH_2 group is brought into a coordinating position by the interaction between the —CHOH— and the metal and that active substrates do not form this type of link.

The structure of the apstatin–*Ec*APPro inhibitor complex provides some structural insight into the specificity of the enzyme, yet it leaves one important question unanswered. The structure shows that the side chain of the N-terminal residue of a substrate fits into a flexible loose pocket that can accommodate a wide range of residues. The hydrophobic nature of this loose pocket is consistent with a slight preference for residues such as phenylalanine and leucine in the N-terminal (P_1) position (Yoshimoto *et al.*, 1994). However, an explanation of the absolute requirement for proline in the second (P_1') position remains elusive. MetAP has an active site closely similar to those of APPro and prolidase. Yet, unlike APPro and prolidase, MetAP can cleave residues with either proline or small uncharged residues in the P_1' position. There do not seem to be any strong specific interactions between the prolidyl rings of Pro residues in the P_1' position and the S_1' binding pockets in the structures of product- or substrate-like inhibitors in complexes with either *Ec*APPro or *Pf*Prol. Indeed, there is not even a perfect correspondence between the proline-residue positions in the apstatin complex of *Ec*APPro and the AHMH-Pro complex of *Pf*Prol, even though the first two residues of the inhibitors are similar and the structures of the S_1' binding pockets are almost identical. The absolute requirement for proline in substrates of *Ec*APPro therefore remains an interesting question for future investigations.

This work is supported by an Australian Research Council grant DP0208320 to HCF and JMG. SCG is the recipient of an Australian Postgraduate Award and MJM is an Australian Research Council Postdoctoral Fellow.

References

Aoyagi, T., Tobe, H., Kojima, F., Hamada, M., Takeuchi, T. & Umezawa, H. (1978). *J. Antibiot.* **31**, 636–638.

Bazan, J. F., Weaver, L. H., Roderick, S. L., Huber, R. & Matthews, B. W. (1994). *Proc. Natl Acad. Sci. USA*, **91**, 2473–2477.

Bhoola, K. D., Figueroa, C. D. & Worthy, K. (1992). *Pharmacol. Rev.* **44**, 1–80.

Brünger, A. T., Adams, P. D., Clore, G. M., DeLano, W. L., Gros, P., Grosse-Kunstleve, R. W., Jiang, J.-S., Kuszewski, J., Nilges, M., Pannu, N. S., Read, R. J., Rice, L. M., Simonson, T. & Warren, G. L. (1998). *Acta Cryst.* D**54**, 905–921.

Copik, A. J., Swierczek, S. I., Lowther, W. T., D'Souza, V. M., Matthews, B. W. & Holz, R. C. (2003). *Biochemistry*, **42**, 6283–6292.

Cruickshank, D. W. J. (1999). *Acta Cryst.* D**55**, 583–601.

Dehm, P. & Nordwig, A. (1970). *Eur. J. Biochem.* **17**, 364–371.

Ersahin, C., Euler, D. E. & Simmons, W. H. (1999). *J. Cardiovasc. Pharmacol.* **34**, 604–611.

Ersahin, C. & Simmons, W. H. (1997). *J. Cardiovasc. Pharmacol.* **30**, 96–101.

Graham, S. C., Lee, M., Freeman, H. C. & Guss, J. M. (2003). *Acta Cryst.* D**59**, 897–902.

Harbeck, H. T. & Mentlein, R. (1991). *Eur. J. Biochem.* **198**, 451–458.

Hirel, P. H., Schmitter, M. J., Dessen, P., Fayat, G. & Blanquet, S. (1989). *Proc. Natl Acad. Sci. USA*, **86**, 8247–8251.

Hooper, N. M., Hryszko, J. & Turner, A. J. (1990). *Biochem. J.* **267**, 509–515.

Jones, T. A., Zou, J. Y., Cowan, S. W. & Kjeldgaard, M. (1991). *Acta Cryst.* A**47**, 110–119.

Keding, S. J., Dales, N. A., Lim, S., Beaulieu, D. & Rich, D. H. (1998). *Synth. Commun.* **28**, 4463–4470.

Kim, K. S., Kumar, S., Simmons, W. H. & Brown, N. J. (2000). *J. Pharmacol. Exp. Ther.* **292**, 295–298.

Kitamura, S., Carbini, L. A., Simmons, W. H. & Scicli, A. G. (1999). *Am. J. Physiol.* **276**, H1664–H1671.

Kleywegt, G. J. & Jones, T. A. (1997). *Methods Enzymol.* **277**, 525–545.

Laskowski, R. A., MacArthur, M. W., Moss, D. S. & Thornton, J. M. (1993). *J. Appl. Cryst.* **26**, 283–291.

Linz, W., Martorana, P. A. & Scholkens, B. A. (1990). *J. Cardiovasc. Pharmacol.* **15** (*Suppl.* 6), S99–S109.

Linz, W., Wiemer, G., Gohlke, P., Unger, T. & Scholkens, B. A. (1995). *Pharmacol. Rev.* **47**, 25–49.

Lowther, W. T. & Matthews, B. W. (2002). *Chem. Rev.* **102**, 4581–4607.

Lowther, W. T., Orville, A. M., Madden, D. T., Lim, S., Rich, D. H. & Matthews, B. W. (1999). *Biochemistry*, **38**, 7678–7688.

McDonald, I. K. & Thornton, J. M. (1994). *J. Mol. Biol.* **238**, 777–793.

Maher, M. J., Ghosh, M., Grunden, A. M., Menon, A. L., Adams, M. W., Freeman, H. C. & Guss, J. M. (2004). *Biochemistry*, **43**, 2771–2783.

Martorana, P. A., Kettenbach, B., Breipohl, G., Linz, W. & Scholkens, B. A. (1990). *Eur. J. Pharmacol.* **182**, 395–396.

Nakamura, H., Suda, H., Takita, T., Aoyagi, T. & Umezawa, H. (1976). *J. Antibiot.* **29**, 102–103.

Otwinowski, Z. & Minor, W. (1997). *Methods Enzymol.* **276**, 307–326.

Prechel, M. M., Orawski, A. T., Maggiora, L. L. & Simmons, W. H. (1995). *J. Pharmacol. Exp. Ther.* **275**, 1136–1142.

Rusu, I. & Yaron, A. (1992). *Eur. J. Biochem.* **210**, 93–100.

Ryan, J. W., Berryer, P., Chung, A. Y. & Sheffy, D. H. (1994). *J. Pharmacol. Exp. Ther.* **269**, 941–947.

Ryan, J. W., Denslow, N. D., Greenwald, J. A. & Rogoff, M. A. (1994). *Biochem. Biophys. Res. Commun.* **205**, 1796–1802.

Schechter, I. & Berger, A. (1967). *Biochem. Biophys. Res. Commun.* **27**, 157–162.

Schneider, T. R. (2002). *Acta Cryst.* D**58**, 195–208.

Simmons, W. H. & Orawski, A. T. (1992). *J. Biol. Chem.* **267**, 4897–4903.

Vanhoof, G., De Meester, I., van Sande, M., Scharpe, S. & Yaron, A. (1992). *Eur. J. Clin. Chem. Clin. Biochem.* **30**, 333–338.

Vaughan, M. D., Sampson, P. B. & Honek, J. F. (2002). *Curr. Med. Chem.* **9**, 385–409.

Vriend, G. (1990). *J. Mol. Graph.* **8**, 52–56.

Wallace, A. C., Laskowski, R. A. & Thornton, J. M. (1995). *Protein Eng.* **8**, 127–134.

Wilce, M. C. J., Bond, C. S., Dixon, N. E., Freeman, H. C., Guss, J. M., Lilley, P. E. & Wilce, J. A. (1998). *Proc. Natl Acad. Sci. USA*, **95**, 3472–3477.

Wolfrum, S., Richardt, G., Dominiak, P., Katus, H. A. & Dendorfer, A. (2001). *Br. J. Pharmacol.* **134**, 370–374.

Yaron, A. (1987). *Biopolymers*, **26** (*Suppl.*), S215–S222.

Yaron, A. & Berger, A. (1970). *Methods Enzymol.* **19**, 521–534.

Yaron, A. & Mlynar, D. (1968). *Biochem. Biophys. Res. Commun.* **32**, 658–663.

Yaron, A. & Naider, F. (1993). *Crit. Rev. Biochem. Mol. Biol.* **28**, 31–81.

Yoshimoto, T., Murayama, N., Honda, T., Tone, H. & Tsuru, D. (1988). *J. Biochem. (Tokyo)*, **104**, 93–97.

Yoshimoto, T., Orawski, A. T. & Simmons, W. H. (1994). *Arch. Biochem. Biophys.* **311**, 28–34.

Zhang, L., Crossley, M. J., Dixon, N. E., Ellis, P. J., Fisher, M. L., King, G. F., Lilley, P. E., MacLachlan, D., Pace, R. J. & Freeman, H. C. (1998). *J. Biol. Inorg. Chem.* **3**, 470–483.

Zhu, P., Zaugg, C. E., Simper, D., Hornstein, P., Allegrini, P. R. & Buser, P. T. (1995). *Cardiovasc. Res.* **29**, 658–663.